

Provided for non-commercial research and education use.
Not for reproduction, distribution or commercial use.



This article appeared in a journal published by Elsevier. The attached copy is furnished to the author for internal non-commercial research and education use, including for instruction at the authors institution and sharing with colleagues.

Other uses, including reproduction and distribution, or selling or licensing copies, or posting to personal, institutional or third party websites are prohibited.

In most cases authors are permitted to post their version of the article (e.g. in Word or Tex form) to their personal website or institutional repository. Authors requiring further information regarding Elsevier's archiving and manuscript policies are encouraged to visit:

<http://www.elsevier.com/copyright>



Contents lists available at ScienceDirect

Remote Sensing of Environment

journal homepage: www.elsevier.com/locate/rse

Mapping canopy conductance and CWSI in olive orchards using high resolution thermal remote sensing imagery

J.A.J. Berni^a, P.J. Zarco-Tejada^{a,*}, G. Sepulcre-Cantó^a, E. Fereres^{a,b}, F. Villalobos^{a,b}^a Instituto de Agricultura Sostenible (IAS), Consejo Superior de Investigaciones Científicas (CSIC), Córdoba, Spain^b Departamento de Agronomía, Universidad de Córdoba (UCO), Córdoba, Spain

ARTICLE INFO

Article history:

Received 9 February 2009

Received in revised form 25 June 2009

Accepted 28 June 2009

Keywords:

Stomatal conductance

CWSI

Water stress

Airborne

UAV

ABSTRACT

The characterization of field properties related to water in heterogeneous open canopies is limited by the lack of spatial resolution of satellite-based imagery and by the physical constraints of point observations on the ground. We apply here models based on canopy temperature estimated from high resolution airborne imagery to calculate tree canopy conductance (G_c) and the crop water stress index (CWSI) of heterogeneous olive orchards. The G_c model requires the simulation of net radiation (R_n) and the aerodynamic resistance (r_a) as a function of windspeed and canopy structure. In both cases, the R_n and r_a models were tested against measurements and published data for olive orchards. Modeled values of G_c of trees varying in water status correlated well with G_c estimates obtained from stomatal conductance measurements in the same trees. The model used to calculate the Crop Water Stress Index (CWSI) took into account, not only the vapor pressure deficit but the R_n and the windspeed as well, parameters known to affect the temperature differences between the air and the tree canopy. The calculated CWSI for water deficit and well irrigated olive trees correlated with the water potential measured on the same trees. The methodology applied in this manuscript was used to validate the estimation of theoretical baselines needed for the CWSI calculations, comparing against traditional empirical baseline determination. High resolution thermal imagery obtained with the Airborne Hyperspectral Scanner (AHS), and from an Unmanned Aerial Vehicle (UAV) for two years was used to map G_c and CWSI of an olive orchard where different irrigation treatments were applied. The methodology developed here enables the spatial analysis of water use within heterogeneous orchards, and the field characterization of water stress, leading to potential applications in the improvement of orchard irrigation management using high resolution thermal remote sensing imagery.

© 2009 Elsevier Inc. All rights reserved.

1. Introduction

The established method for detecting water stress of crops in the field uses a pressure chamber to measure the xylem water potential of individual leaves in selected plants (Hsiao, 1990; Shackel et al., 1997). Another water stress indicator is based on measuring stomatal conductance with leaf diffusion porometers. Both methods provide point observations which are not free of measuring errors (Hsiao, 1990) and are very time consuming, limiting the number of individuals that can be monitored to accurately characterize a field. Water stress induced stomatal closure reduces transpiration rate, thus reducing evaporative cooling and increasing leaf temperature that could be tracked by thermal infrared thermometers and imagers. This approach at detecting

water stress became very popular in the 1970's and 80's with the advent of hand-held thermometers (Tanner, 1963; Fuchs & Tanner, 1966; Idso et al., 1978; Idso et al., 1981; Jackson et al., 1977a,b; Jackson et al., 1981; Jackson, 1982) and led to the development of a normalized index to overcome the effects of other environmental parameters affecting the relation between stress and plant temperature. The index was termed the Crop Water Stress Index (CWSI) (Idso et al., 1981; Jackson et al., 1981), and consisted in relating the actual difference between canopy and air temperatures (T_c and T_a , respectively) to the difference between the $T_c - T_a$ values of a non-water stressed baseline (NWSB), and an upper $T_c - T_a$ limit, both being a function of the atmospheric vapor pressure deficit (VPD) (Idso et al., 1981). A CWSI ranging from 0 to 1 is thus obtained which was found to be proportional to the stress level in many crops, provided that NWSB values are known for the crop and local conditions. Many NWSB equations were published in the past for different crops (Idso, 1982; Nakayama & Bucks, 1983; Glenn et al., 1989; Wanjura et al., 1990; Sepaskhah & Kashefipour, 1994; Yazar et al., 1999; Testi et al., 2008). A major reason for the interest in the CWSI was the possibility of measuring it remotely, thus avoiding time consuming techniques used for detecting stress at the field or farm levels.

* Corresponding author. Instituto de Agricultura Sostenible (IAS) Consejo Superior de Investigaciones Científicas (CSIC), Alameda del Obispo, s/n, 14004, Córdoba, Spain. Tel.: +34 957 499 280, +34 676 954 937; fax: +34 957 499 252.

E-mail address: pzarco@ias.csic.es (P.J. Zarco-Tejada).

URL: <http://quantalab.ias.csic.es> (P.J. Zarco-Tejada).

However, the use of CWSI as a stress indicator has not been widely adopted for two main reasons (Cohen et al., 2005): (i) temperature remotely sensed from readily available satellite platforms or airborne sensors lacks the necessary spatial resolution for the accurate separation of canopy temperature from the sunlit and shaded soil background; (ii) the different equations of NWSB published are site dependent, since the VPD normalization procedure used for obtaining the CWSI does not account for differences in net radiation and aerodynamic resistance which are known to affect the index (Hipps et al., 1985; Jackson et al., 1988; Jones, 1999). Avoiding the first issue is not easy, since currently available satellite thermal imagery is limited to Landsat TM and ASTER scanners, yielding 120 m and 90 m, respectively, and MODIS or AVHRR, with 1 km pixel size. The medium-low spatial resolution of such satellite thermal scanners makes mapping water stress only potentially suitable for regional scales if successfully accounting for canopy heterogeneity (Moran et al., 1994; Norman et al., 1995). Alternatively, airborne thermal imagery has been proved suitable for mapping water stress on discontinuous canopies (Sepulcre-Canto et al., 2006; Sepulcre-Canto et al., 2007), provided that the spatial resolution allows the detection of isolated tree crowns (<2 m pixel size). However, the cost and operational complexity of airborne platforms make its extensive use in agriculture very limited (Berni et al., in press). New thermal imaging sensors onboard unmanned aerial platforms provide sub-meter spatial resolution (Herwitz et al., 2004; Sugiura et al., 2005; Berni et al., 2009) enabling the retrieval of pure canopy temperature, thus minimizing soil thermal effects. High resolution thermal imagery would make possible the retrieval of energy fluxes from pure vegetation on open canopies, such as tree orchards, where most remote sensing based methodologies do not perform well. Nevertheless, atmospheric effects and atmospheric transmittance should be considered even for low altitude platforms aimed at keeping temperature measurement errors below 1 K (Berni et al., 2009).

If high resolution canopy temperature can be accurately monitored then the extensive use of CWSI may be a practical option. New theoretical and practical approaches have been proposed to overcome the need for the empirical retrieval of the NWSB needed in the CWSI calculation. The use of theoretical equations of CWSI based on the energy balance equation (Jackson et al., 1988) is limited by the need to estimate net radiation and aerodynamic resistance, but it allows the calculation of canopy conductance (Smith, 1988; Leinonen et al., 2006; Lhomme & Monteny, 2000). Most recent works overcome this problem by using dry and wet references that account for the CWSI upper and lower limits, respectively, allowing the estimation of CWSI with a minimum of meteorological measurements (Jones et al., 2002; Cohen et al., 2005; Grant et al., 2007; Möller et al., 2007). However the use of such reference surfaces is a clear limitation for the practical and extensive use of this methodology.

This manuscript validates a methodology to map the spatial distribution of CWSI and the canopy conductance of a field from very high spatial resolution thermal imagery and *in situ* atmospheric variables. This approach is particularly suitable for monitoring areas of medium size (in the order of hundred of hectares) using unmanned aircrafts that could provide frequent visits and short turnaround times to detect water stress for irrigation scheduling. The methodology presented here does not require the use of reference surfaces and relies on physical models to estimate all input variables of the energy balance equations.

2. Model approach for estimating canopy conductance

The model departs from the assumption that pure vegetation surface temperature can be retrieved from thermal imagery if the spatial resolution enables to discriminate pure crown pixels from sunlit and shadowed soil pixels. Furthermore, *at-sensor* radiometric temperature is converted to surface temperature by means of atmospheric and emissivity corrections.

Assuming that the energy stored in the foliage and the energy used in the photosynthetic processes are negligible, the energy balance in the canopy foliage is written as:

$$R_n^c = H_c + \lambda E_c \quad (1)$$

where R_n is the net radiation, H_c the sensible heat flux into the air, and λE is the latent heat flux. The subscript c denotes that only the canopy energy fluxes are considered.

The terms H_c and λE_c can be expressed as:

$$H_c = \rho C_p \cdot \frac{(T_c - T_a)}{r_a} \quad (2)$$

$$\lambda E_c = \frac{\rho \cdot C_p \cdot (e_c^* - e_a)}{\gamma \cdot (r_a + r_c)} \quad (3)$$

where ρ is the air density; C_p the specific heat of air; T_c and T_a are respectively the temperature of the canopy and air; and r_a is the aerodynamic resistance; e_c^* is the saturated vapor pressure at the canopy temperature; e_a is the actual vapor pressure of air; γ the psychrometric constant; and r_c is the canopy resistance to vapor transport.

Combining Eqs. (1)–(3), r_c is calculated as:

$$r_c = \frac{r_a(e_c^* - e_a)}{\gamma \left(\frac{r_a R_n}{\rho C_p} - (T_c - T_a) \right)} - r_a \quad (4)$$

To solve this equation, T_a and e_a can be retrieved from a weather station whereas ρC_p and γ are calculated from T_a and atmospheric pressure. T_c can be measured by means of thermal infrared sensors, or in a larger scale it is obtained from thermal imagery. Although net radiation can be measured locally using a net radiometer, this instrument is not generally available and a parameterization is needed to estimate net radiation from local weather variables, as presented below. Also, aerodynamic resistance depends mainly on wind speed and canopy structure, but it is also affected by buoyancy effects when $T_c > T_a$ and needs to be modeled based on weather parameters. The accuracy of the estimated canopy conductance is function of the input parameters used, with some authors providing sensitivity analyses for these parameters. They remark the importance of the errors in net radiation, temperature and vapor pressure deficit [Leinonen et al., 2006] but also the importance of aerodynamic resistance in water stressed crops [Rana & Kterji, 1998].

2.1. Net radiation modeling

The radiation balance over the foliage can be described as:

$$R_n = (1 - \alpha_c) \cdot R_s^{\downarrow} - \varepsilon_c \cdot \sigma \cdot T_c^4 + \varepsilon_c \cdot R_L^{\downarrow} \quad (5)$$

where R_n is the net radiation, α_c is the total shortwave surface albedo; R_s is the solar shortwave irradiance; ε_c is the surface broadband emissivity; σ is the Stefan–Boltzmann constant; and R_L^{\downarrow} is the longwave incoming irradiance from the atmosphere. In this equation R_s can be measured by means of a pyranometer, available in most of the agro-meteorological weather stations, the broadband emissivity for pure vegetation can be assumed as 0.98 (Monteith & Unsworth, 2008; Salisbury & D'Aria, 1992). However, special attention must be paid to surface albedo and incoming longwave radiation.

Downwelling longwave radiation can be measured with longwave radiometers (pyrgeometers), which are rare in weather stations. An alternative is the use of radiative transfer models such as MODTRAN (Berk et al., 1999) but a good knowledge of the atmospheric profile is required. Several methods have been developed during the past century in order to estimate R_L^{\downarrow} from surface weather variables with reasonable

results (for a review see Crawford & Duchon, 1999). These techniques are based on the Stefan–Boltzmann law, using the effective emissivity and temperature of the overlying atmosphere according to:

$$R_L^{\downarrow} = \varepsilon_{\text{atm}} \cdot \sigma \cdot T_{\text{atm}}^4 \quad (6)$$

Given the difficulty to estimate ε_{atm} and T_{atm} , the developed methods parameterize R_L^{\downarrow} from the measured air temperature and vapor pressure at surface level. Several authors have published relationships of sky emissivity for clear days ($\varepsilon_{\text{clear}}$) as a function of T_a and/or vapor content (see review by Kjaersgaard et al., 2007). Most of these models have been developed with specific datasets from a region which limits its general use. An additional problem occurs when non-clear sky conditions are present, since the presence of clouds and aerosols increases R_L^{\downarrow} . A solution proposed by Crawford and Duchon (1999) is the use of the cloud fraction term (*clf*) to correct the emissivity on clear conditions, defining *clf* as

$$\text{clf} = 1 - s \quad (7)$$

where *s* is the fraction of the measured shortwave irradiance over the potential clear sky irradiance, which can be estimated by radiative transfer models like MODTRAN (Berk et al., 1999) used in this study.

$$R_L^{\downarrow} = [\text{clf} + (1 - \text{clf}) \cdot \varepsilon_{\text{clear}}] \cdot \sigma \cdot T_{\text{atm}}^4 \quad (8)$$

The emissivity for clear days has been calculated using the model proposed by Brutsaert (1975) and adapted by Crawford and Duchon (1999).

Surface albedo can be measured directly by albedometers over the surface of interest, which is not operational for larger-scale applications. Since broadband albedo can be defined as the integration of the reflectance for all the wavelengths of the shortwave spectrum, some authors proposed the use of discrete bands from multispectral imaging sensors (Brest & Goward, 1987; Liang, 2001) using weighting coefficients for each specific band. Broadband albedo depends not only on the surface characteristics but also on atmospheric conditions such as turbidity and cloudiness, and the solar zenith angle. For clear days, the main driver for albedo is the solar zenith angle (Liang, 2001). Therefore if albedometer measurements are available for a number of clear sky days, the albedo can be determined as a function of the solar zenith angle.

2.2. Aerodynamic resistance modeling

Aerodynamic resistance becomes a very important parameter in the energy balance equations when estimating sensible heat flux and latent heat flux using remote sensing measurements. Many authors have published different parameterizations to model aerodynamic resistance with different levels of simplification and empiricism (see review in Liu et al., 2007).

In this study, the model of Viney (1991) has been used given the simplicity of that parameterization and good results according to Liu et al. (2007). That model is valid for stable and non-stable conditions, which are very common in olive tree orchards in summer, where the canopy temperature can be several degrees above the air temperature.

The zero plane displacement (*d*) and the roughness lengths (z_0), which depend on canopy dimensions and architecture, can be estimated using wind profiles and momentum flux measurements. However very simple empirical functions of canopy height (*h*) have been proposed, such as $d=0.66$ h and $z_0=0.13$ h (Brutsaert, 1982; Monteith & Unsworth, 2008). Nevertheless, these values were proposed for uniform cropping surfaces or dense forests with a closed canopy, and may not apply to sparse and heterogeneous canopies. Verhoef et al. (1997) demonstrated that Raupach's analytical treatment of drag and drag partition on rough surfaces using dimensional analysis performed well even on sparse canopies, and that values of *d/h* and z_0/h could be

obtained as a function of the frontal area index and the canopy structure. We have applied Raupach's methodology to the study site and the following relationships were obtained: $d=0.732$ h and $z_0=0.113$ h. These values are close to the values given by Monteith and Unsworth (2008) and Brutsaert (1982), and are also in accordance with those obtained by Villalobos et al. (2000) for an olive orchard.

2.3. Modelling CWSI

An analytical solution for the CWSI may be obtained once that r_c and the potential canopy resistance for a non-water stressed crop (r_{cp}) are known (Jackson et al., 1981):

$$\text{CWSI} = 1 - \frac{E}{E_p} = \frac{\gamma(1 + r_c/r_a) - \gamma^*}{\Delta + \gamma(1 + r_c/r_a)} \quad (9)$$

where Δ is the slope of the saturation vapor pressure temperature relationship and,

$$\gamma^* = \gamma(1 + r_{cp}/r_a) \quad (10)$$

Since r_c can be calculated from Eq. (4) using the methodology described above, a CWSI map could be generated from high spatial resolution thermal imagery. The method would require *in situ* meteorological measurements and physical models used to estimate R_n and r_a . As the spatial resolution used in this study (40 cm pixel size) enables isolating the tree crown temperature from the soil background, there is no need for using vegetation indices to estimate the fraction vegetation cover as required in ET models (see Moran et al., 1994). Additionally, the proposed methodology based on physical models does not require the need for a reference surface, as proposed on recent studies for CWSI estimation (Jones et al., 2002; Cohen et al., 2005; Grant et al., 2007; Möller et al., 2007).

Estimates of r_{cp} has been published for many crops, also for the case of olive trees (Morianana et al., 2002; Testi et al., 2006). Additionally, theoretical models of canopy resistance may be used to estimate this parameter, e.g. Jarvis (1976).

3. Materials and methods

3.1. Field data collection

The study site was located in southern Spain, consisting on a 4-ha olive orchard (*Olea europaea* L cv. 'Arbequino') planted at 7.0×3.5 m, with rows oriented in the NS direction, an average crown height of 5 m and a leaf area index (LAI) of 1.4 when the measurements were performed. Therefore, the LAI within the area covered by the tree crowns would be over 3.0, a value found in most annual crops to ensure almost full radiation interception by the canopy (Ritchie, 1972).

The climate of the area is Mediterranean with an average annual rainfall of 650 mm, concentrated from autumn to spring, and a reference evapotranspiration of 1390 mm. This olive orchard has been the site for previous ET and irrigation-related studies (Iniesta et al., 2009; Testi et al., 2004; Moriana & Fereres, 2002). The experiment monitored had three different drip-irrigation treatments within an area of 6 rows of 18 olive trees each (2646 m²). The treatments were: i) a control (FI) that applied 2.8 mm/day equivalent to full ET; ii) a sustained deficit irrigation (SDI) that applied 0.7 mm/day or 25% of FI; and iii) a regulated deficit irrigation (RDI) treatment which applied, 1.2 mm/day from 14 June to 5 July and from 6 September to 19 October, and no irrigation from 5 July to 6 September (see Iniesta et al., 2009).

Ten infrared temperature (IRT) sensors (model IRTS-P, Apogee, Logan, UT, USA) were placed 1 m above the trees from the three irrigation treatments (Sepulcre-Canto et al., 2006), recording the mean temperature at 5-minute intervals in 3 dataloggers (model

CR10X, Campbell Sci., Logan, UT, USA). Two additional sensors were placed over bare soil, recording temperature at the same time intervals over sunny and shaded soil. Air temperature and humidity were measured above the canopy with an air temperature and humidity probe (model HMP45C, Vaisala, Helsinki, Finland) placed 1 m above the canopy (approx. 6 m above the ground).

A high precision albedometer (model CM7B, Kipp & Zonen, Delft, NL) and a net pyrometer (model CG2, Kipp & Zonen, Delft, NL) were installed 1 m above one tree to measure continuously downward and upward shortwave and longwave radiation fluxes to calculate surface albedo. Weather data were retrieved from an automated weather station located on an irrigated grass (*Festuca arundinacea* L.) plot of 1.5 ha, situated 500 m east of the olive orchard. Data was recorded on a 10-minute basis, including wind speed and direction at 2 m height, air temperature and humidity at 1.5 m, and solar radiation.

Leaf stomatal conductance was measured weekly around 10:30 GMT during the summer of 2005, and on 23 August, 2007 at 13:30 GMT with a steady-state porometer (model PMR-4, PP Systems, Hitchin Herts, Great Britain). On every one of the 10 monitored trees, 5 well illuminated and fully expanded, middle aged leaves were selected and identified in order to do the measurements on the same leaves during 2005, while different leaves were selected in 2007. It is well known that scaling up leaf measurements of stomatal conductance to canopy conductance is not straightforward (Baldochi et al., 1991; Lhomme, 1991; Furon et al., 2007). Here, we assumed that the measured canopy resistance was represented by the resistance of the population of sunlit leaves with their measured resistances in parallel. For this reason only sunlit leaves were measured with the porometer, and the average leaf resistance measurements were compared against the estimates of canopy conductance calculated with the model (Eq. (4)).

Leaf water potential was measured on the monitored trees with a pressure chamber (PWSC Model 3000, Soilmoisture equipment Corp., California, USA) on 26 August, 2007 at 13:30 GMT, following the procedure described in Sepulcre-Canto et al. (2006).

3.2. Airborne campaigns

An airborne campaign was conducted by the Spanish Aerospace Institute (INTA) with the Airborne Hyperspectral Scanner (AHS). The AHS sensor was flown over the olive orchard at 3 different times (7:30 GMT, 9:30 GMT, 12:30 GMT) on 16 July 2005 at 1000 m altitude above ground level (AGL), obtaining 6000×2000 m² images at 2 m spatial resolution (Fig. 1a). The AHS sensor has 80 spectral bands in the 0.43–12.5 μm spectral range. The 80 bands are distributed in 4 spectral regions (VIS/NIR, SWIR, MWIR and TIR) with a field of view (FOV) of 90° and a 2.5 mrad instantaneous field of view (IFOV). A full description of the AHS bands, calibration methods, and the radiometric and atmospheric correction procedures can be found in Sobrino et al., (2006).

Another set of images were collected from an unmanned aerial vehicle (UAV) platform which was developed to carry a payload with thermal and multispectral imaging sensors for remote sensing operation (Berni et al., 2009). The study site was scanned with the UAV carrying a thermal camera on 23 August 2007 at an altitude of 150 m AGL (Fig. 1b). The thermal imager used was the Thermovision A40 M (FLIR, USA). The image sensor is a Focal Plane Array (FPA) based on uncooled microbolometers with a resolution of 320×240 pixels, 38×38 μm pixel size and spectral response in the range of 7.5–13 μm, yielding a sensitivity of 0.08 K at 303 K. The camera was equipped with a 40° FOV lens, which delivered 40 cm spatial resolution imagery at the flight altitude, enabling the retrieval of pure crown temperature from each tree under study (Fig. 1c).

Airborne AHS and UAV thermal imagery were processed applying geometric, radiometric and atmospheric corrections. AHS image atmospheric correction was conducted using the MODTRAN-4 radiative transfer code (Berk et al., 1999). *In situ* atmospheric profiles were conducted at 7:00 and 12:00 GMT on 16 July 2005 for AHS atmospheric

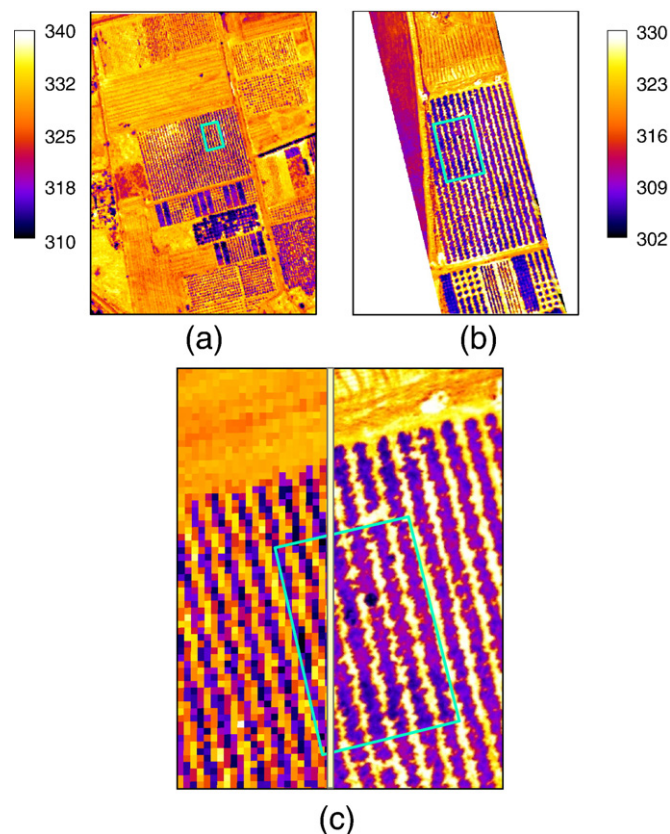


Fig. 1. Airborne thermal imagery acquired over the study site: a) AHS image collected at 12:30GMT on 16 July 2005; b) UAV image collected at 13:30 GMT on 23 August 2007; c) image detail showing the spatial resolution differences of AHS (2 m) against the UAV (40 cm). The spatial resolution of the UAV imagery shows individual tree crown, enabling pure crown temperature extraction.

correction. Land surface temperature (LST) was retrieved from AHS thermal infrared data acquired in 2004 and 2005 using the split-window algorithm described in Sobrino et al. (2006). For the UAV imagery, surface temperature was obtained applying atmospheric correction methods based on the MODTRAN radiative transfer model. Local atmospheric conditions such as air temperature, relative humidity and barometric pressure were measured at the time of flight with a portable weather station (Model WXT510, Vaisala, Finland) and used as input into MODTRAN. A single-layer atmosphere with uniform conditions was considered for the simulations since the variation for the typical UAV flight altitude (150–200 m) could be neglected. Optical path transmissivity and thermal radiance were calculated for every pixel on the image, taking into account the flight elevation and the effects introduced by the wide field of view and camera tilt angles. Additionally, the mosaicking process selects only the most nadir part of the overlapping images, limiting the viewing angle and thus avoiding directional effects and thermal hotspot. The atmospheric correction methods showed a RMSE <1 K in a validation with ground measured temperature over three different targets at different times of the day (Berni et al., 2009).

4. Results and discussion

4.1. Model performance

Data from the albedometer on clear days was plotted for different solar zenith angles (θ) resulting in a relationship between $\cos(\theta)$ and albedo (Eq. (11)) with $R^2 = 0.83$ and a RMSE = 0.044:

$$\alpha_c = 0.1268 \cdot \cos(\theta)^{-0.4356} \quad (11)$$

Downwelling longwave radiation was estimated using e_a and T_a to calculate the clear sky atmospheric emissivity. The cloudiness factor (clf) was calculated using the measured shortwave radiation and the estimated potential irradiance. However, poor results were obtained when the cloudiness factor was applied with the 10-minute interval dataset; using a daily average clf improved estimates, even on almost-clear days (RMSE = 7.96 W/m², MBE = -0.78 W/m²). Finally, net radiation was estimated for a number of selected dates and compared with the direct measurements from the albedometer and net pyrgometer, showing a good fit between estimated and measured net radiation (RMSE = 22.53 W/m², MBE = 9.04 W/m²).

Aerodynamic resistance was calculated using 10-minute data with the methodology proposed in Section 2.2. Canopy temperature and meteorological data were used to calculate H_c and λE_c by means of Eqs. (2) and (3), showing in Fig. 2 the calculations for the day of the AHS airborne flight (197). As expected, fully irrigated trees showed higher λE_c and lower H_c as compared with the deficit irrigation trees. Fig. 2b shows RDI and SDI treatments, observing that λE_c starts to decline soon after 8:00 GMT with a strong reduction after noon, while λE_c fluxes for the FI trees were maintained all along the midday, starting to decrease when net radiation was reduced. For G_c , canopy resistance was calculated using Eq. (4), deriving G_c as the inverse of r_c (Monteith & Unsworth, 2008). The diurnal course of canopy conductance curve for each treatment (Fig. 3) reflects a pattern similar to the response as a function of water deficits of olive stomata shown in Moriana et al. (2002), and to the G_c behavior reported in Villalobos et al. (2000) and in Orgaz et al. (2007). The pattern shows a sudden increase in G_c early in the morning, a progressive decline as a result of stomata closure during the central hours of the day, and very low values with the absence of solar radiation at the end of the day. Fig. 3 also depicts the effects of water deficits on G_c values of each treatment, showing that deficit irrigated trees closed stomata sooner than the control trees as their canopy conductance values were lower, even approaching to zero after midday.

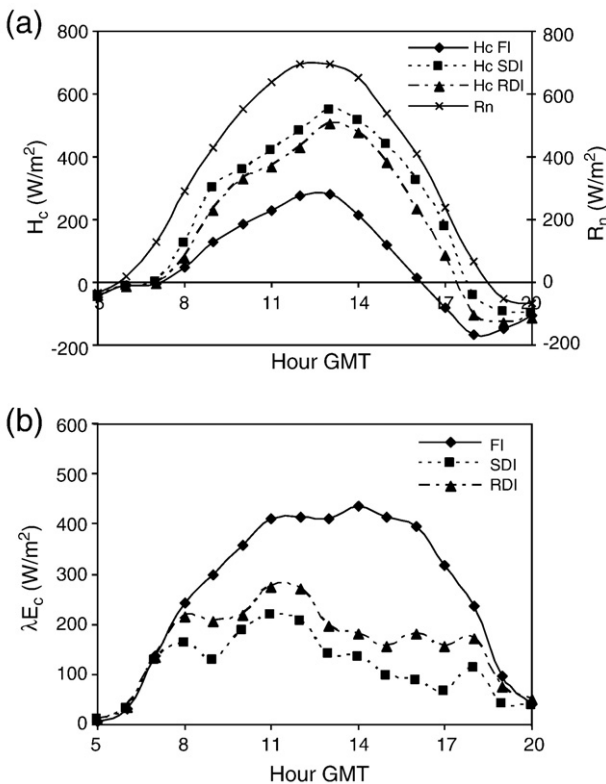


Fig. 2. Diurnal course of net radiation (R_n), sensible heat (H_c) and latent heat (λE_c), hourly averaged for each treatment on DOY 197.

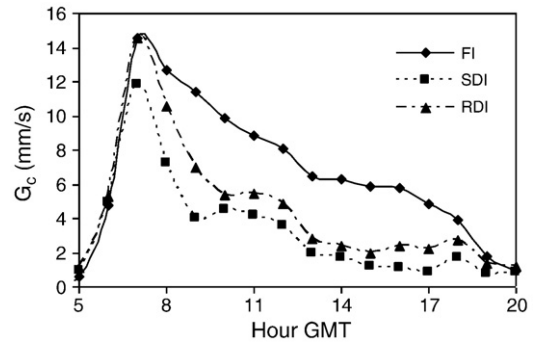


Fig. 3. Hourly averaged estimations for simulated canopy conductance on DOY 197 using Eq. (4).

Fig. 4 shows the behavior of the estimated G_c at noon during summer 2005 for each treatment, observing that full irrigated trees (FI) yielded greater G_c compared with the deficit irrigated trees (RDI and SDI), reaching the maximum differences during mid July to August. Three arrows (shown in Fig. 4) indicate rainfall events that took place during summer 2005, noting after each rain event the increase in G_c , especially after May 12 (day of the year 132).

4.2. Model validation using ground thermal sensors

Two tests were conducted to assess the performance of the model against measurements with IRT sensors: a) comparing model estimates against canopy conductance measurements at different times from a single day; and b) comparing the model estimates for different dates at noon along summer 2005. Single day model estimates presented on Fig. 5a show a relationship with $R^2 = 0.63$ (slope = 1.17 and intercept = 1.05) and a RMSE = 2.63 mm/s. In the case of the validation for different dates, shown on Fig. 5b, the determination coefficient ($R^2 = 0.68$) suggests a reasonable model performance for different weather conditions. A large scatter for estimated G_c was found for low values of measured conductance. This could be explained by the large variability inherent to the leaf porometer measurement method and the scaling up from leaf to canopy levels. The assumption made was that the measured leaves represent the average population of the whole tree; however, since only a limited number of leaves can be measured for each tree, the resulting G_c could differ from the actual tree G_c . Unfortunately, measuring a larger number of leaves per tree, within a short time, is not possible for leaf porometry and therefore other methods, such as trunk sap flow or eddy covariance should be used to estimate actual G_c , which deserves further research. Nevertheless, these results suggest that thermal monitoring using point IRT sensors could be used to track canopy conductance and latent heat flux on isolated trees.

4.3. Model validation using airborne remote sensing thermal imagery

The proposed methodology was applied to airborne thermal calibrated imagery collected in 2005 and 2007 campaigns. The required inputs for the model, latitude, longitude, day of the year and GMT time, enabled the calculation of net radiation for clear days; air temperature and relative humidity, actual solar radiation from the pyranometer and wind speed over grass. Canopy height, reference height, z_0/h and d/h can also be introduced in order to model the aerodynamic resistance. The 2 m resolution AHS thermal imagery was processed using an NDVI mask to extract pure crown temperature (as explained in Sepulcre-Canto et al. (2006)) at the three times of day when the sensor was flown: 7:30, 9:30, and 12:30 GMT. The algorithm was applied to the masked images, estimating canopy conductance for each individual tree. Fig. 6 shows the validation of the estimated values

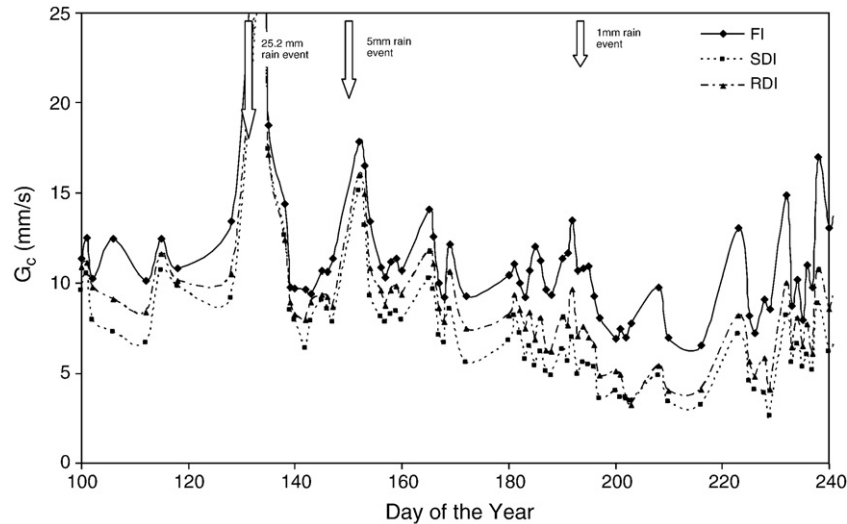


Fig. 4. Seasonal variation of canopy conductance (G_c) for the three different irrigation treatments obtained from the infrared sensor temperature at 12:00GMT during summer 2005.

versus the field-measured G_c , showing that the estimations for 7:30 and 9:30 GMT are close to the 1:1 line with a RMSE of 2.25 and 1.80 mm/s, respectively. However, the estimation conducted from the 12:30 GMT flight resulted in an overestimation of G_c as compared to the field measurements. The expected behavior would be an underestimation of G_c or even negative values as a consequence of the surrounding warm soil and pixel mixing. However, the good correlation between the estimated and the measured G_c values

($R^2 = 0.59$), suggests a bias in the radiometric calibration or atmospheric correction of the AHS thermal imagery.

For the higher spatial resolution UAV thermal imagery acquired in 2007 summer campaign, individual tree crowns were delineated clearly due to the higher spatial resolution of the imagery (40 cm pixel size). The resulting estimated canopy conductance image (Fig. 7) shows the well watered trees (FI treatment) with higher canopy conductance, with lower G_c values corresponding to deficit irrigated trees (RDI and SDI treatments). Single-tree estimated G_c values were manually extracted from the imagery, identifying the trees where field measurements were conducted. The validation of the estimated G_c values (Fig. 8) shows a very good relationship ($R^2 = 0.91$) and a slope close to 1 (1.08) with an intercept of 0.84 mm/s (RMSE = 1.65 mm/s). Additionally, the results show less scatter than those obtained from AHS thermal imagery, suggesting that higher spatial resolution is critical for an accurate extraction of pure crown canopy temperature and to avoid energy fluxes from the bare soil.

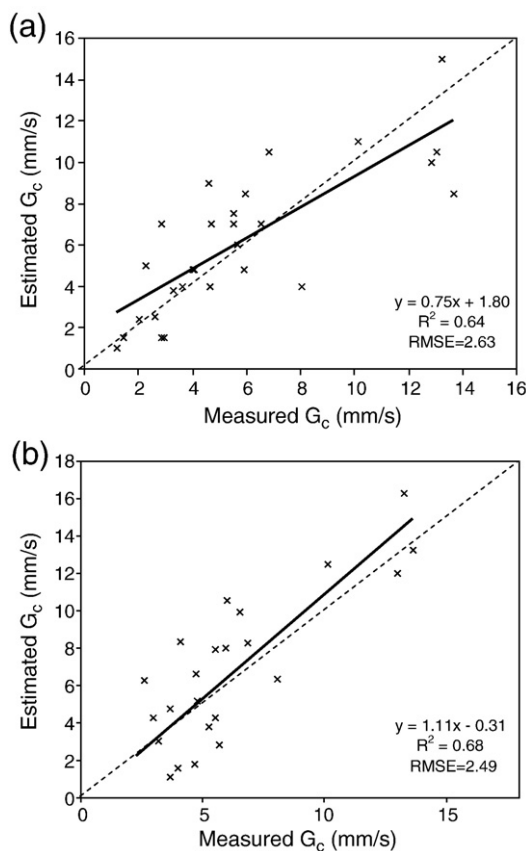


Fig. 5. Relationship obtained between the measured canopy conductance (G_c) and the estimated G_c for a) individual tree measurements at three times (7:30GMT, 9:30GMT and 12:30GMT) on 16 July 2005 ($n = 30$), and b) treatment averages during summer of 2005 ($n = 25$).

4.4. Mapping CWSI at high resolution in open-canopy orchards

To calculate the theoretical CWSI using Eq. (9), the crop potential canopy conductance in the absence of water stress should be known, which for olive trees is a strong function of VPD (Moriani et al., 2002; Testi et al., 2006). In this study, in order to determine the function of

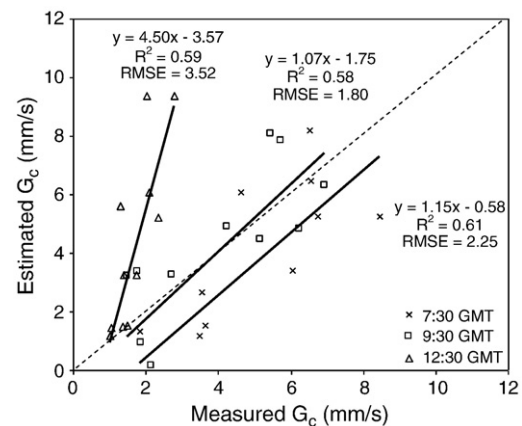


Fig. 6. Relationship obtained for the field-measured leaf stomatal conductance and from the AHS imagery estimates for individual trees at the different times (7:30GMT, 9:30GMT and 12:30GMT) on DOY 197, 2005.

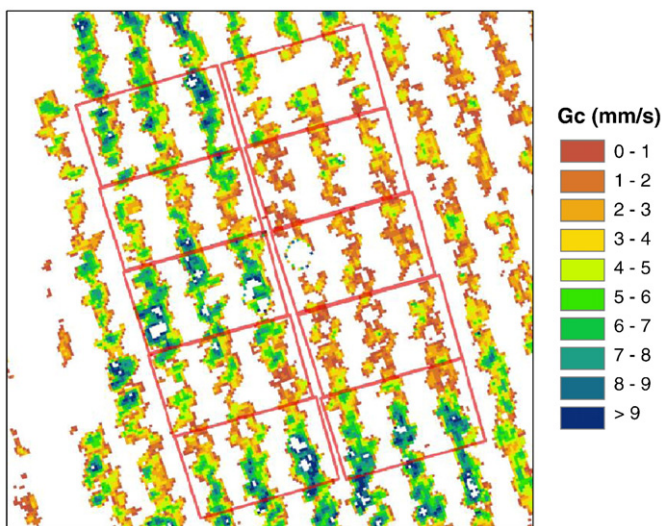
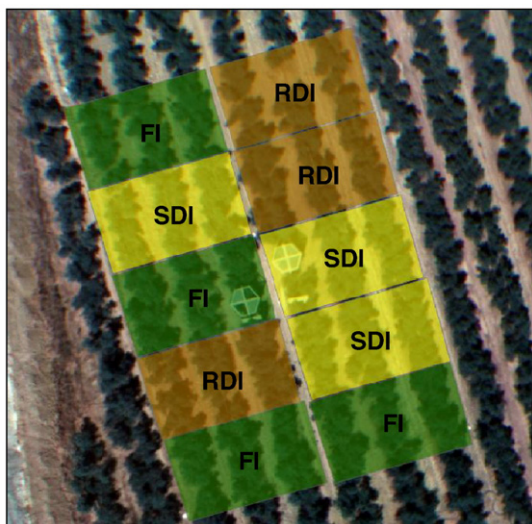


Fig. 7. Canopy conductance map obtained from the UAV thermal imagery at 13:30 GMT 23 August 2007. Units are mm/s. Local conditions were $T_a = 304.16$ K, $RH = 19.69\%$, $U_g = 1.2$ m/s.

canopy potential conductance (G_{cp}) as a function of the VPD , full irrigation trees were monitored and the estimations of G_c at noon on clear days with summer standard conditions ($R_n = 700$ W/m²) were

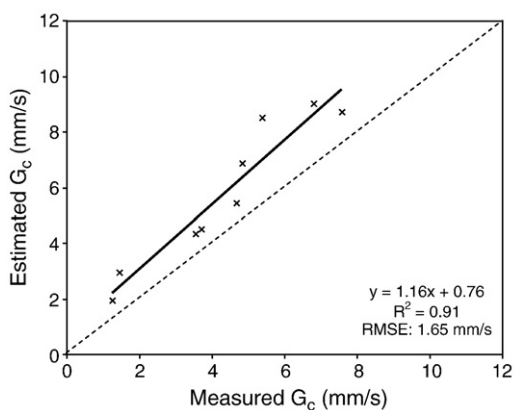


Fig. 8. Validation of the canopy conductance estimations against field measurements. Each point shown represents an individual tree where 5 stomatal conductance measurements were taken.

plotted against the VPD , yielding a close relationship ($R^2 = 0.7$) and the following equation:

$$G_{cp} = 25.533 \cdot VPD^{-0.7437} \quad (12)$$

CWSI was calculated using the estimated G_c from the air using the high resolution airborne imagery acquired in 2007 and the resulting G_{cp} from the meteorological conditions at the time of the flight, obtaining a CWSI map with values ranging from 0 to 1 (Fig. 9). The value of CWSI was extracted for the trees where leaf water potential was measured. Fig. 10 delineates the relationships between CWSI and leaf water potential (a) and canopy conductance (b) showing strong correlations ($R^2 = 0.82$ and $R^2 = 0.91$ respectively), which suggests that CWSI obtained from high spatial resolution thermal imagery can be used as a good indicator to map water stress in open tree canopies. Compared with a map of G_c , the main advantage of a CWSI map is that absolute values of G_c cannot be directly translated as an indicator of water stress, whereas CWSI may be used as a stress indicator because it is already normalized for weather conditions and crop characteristics.

As indicated earlier, a major goal would consist on assessing the proposed modeling methodology to calculate the theoretical NWSB using analytical equations. The $T_c - T_a$ value was calculated iterating Eq. (13) as function of VPD with the following average conditions for the summer in Cordoba: $R_n = 700$ W/m² and 650 W/m², $T_c = 32$ °C, $U_g = 2.24$ m/s and $U_g = 1.5$ m/s.

$$T_c - T_a = \frac{r_a R_n}{\rho C_p} \cdot \frac{\gamma(1 + r_c/r_a)}{\Delta + \gamma(1 + r_c/r_a)} - \frac{VPD}{\Delta + \gamma(1 + r_c/r_a)} \quad (13)$$

Additionally, the non-water-stressed baseline (NWSB) was obtained empirically using the $T_c - T_a$ values for the trees of the FI treatment (fully irrigated) close to solar noon (12:30 GMT, AHS sensor flight time) using hourly averaged values from clear days from April to September 2005 (days of the year 100–252) were used. The calculated NWSB ($T_c - T_a = -0.35 \cdot VPD + 2.08$, $R^2 = 0.67$) showed large scatter and a very small slope compared with reported baselines from other authors. This means that for large variations of VPD , $T_c - T_a$ varies less than 1.5 K, which is a very small difference if compared with NWSB for herbaceous crops but also for some tree species such as pistachio (Testi et al., 2008). This is a consequence of the small leaves of the olive which are highly coupled to the atmosphere (Villalobos et al., 2000), and also because even for well irrigated trees, some stomatal closure occurs when the evaporative demand increases. A consequence of this very small slope is

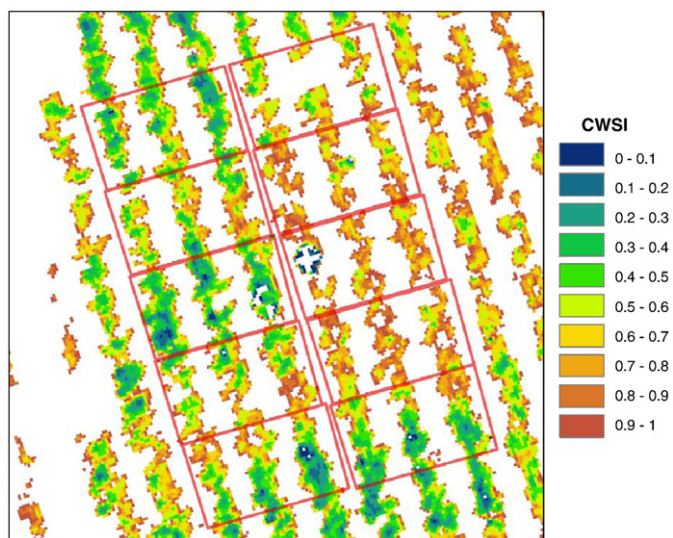


Fig. 9. CWSI map obtained from the UAV high resolution thermal imagery at 13:30 GMT on 23 August 2007.

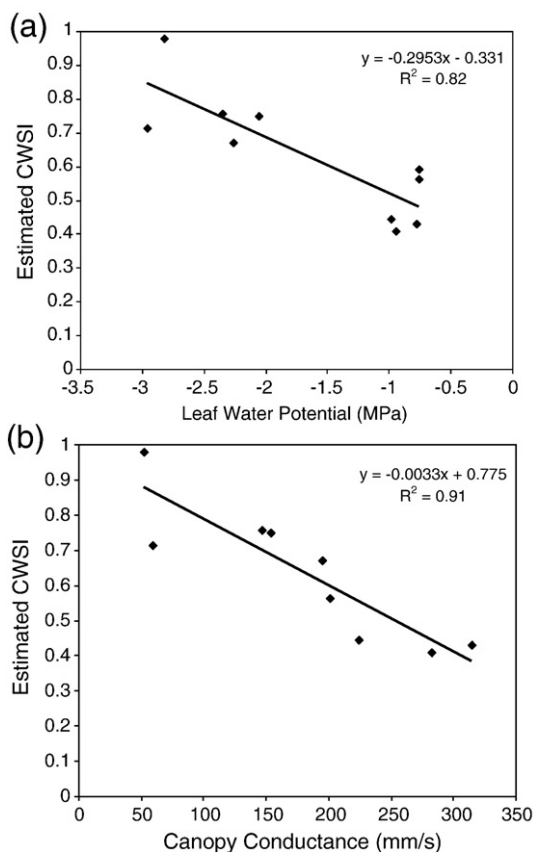


Fig. 10. Relationships between the estimated CWSI from the UAV thermal imagery with a) leaf water potential and b) canopy conductance.

that CWSI for olive trees is very sensitive to errors in the estimation of T_c and the measurement of T_a .

Fig. 11 shows the resulting NWSB simulations as compared with the empirical NWSB (solid line). The plot agrees with the theoretical estimates of Hipps et al. (1985) and with the experimental results of Testi et al. (2008) who determined NWSB lines for pistachio, where the variations in radiation caused by time of day also resulted in parallel baselines. This suggests that the model formulated in the present paper could be used to determine NWSB without the limitations of local conditions and the empiricism involved in the original methodology of Idso et al. (1981). Although the traditional NWSB approach is still useful, the methodology proposed here could be used to generate baselines for different conditions and crops to be used by farmers applying CWSI as an irrigation scheduling technique.

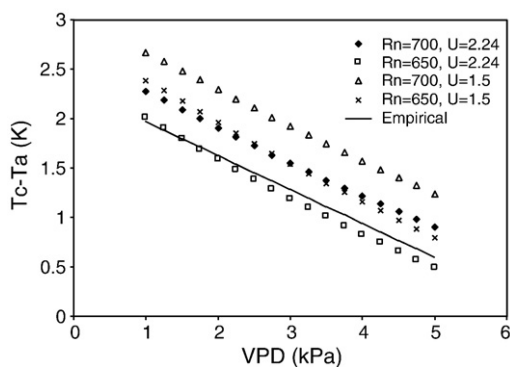


Fig. 11. Simulations of NWSB for CWSI from 4 weather conditions: $R_n = 600 \text{ W/m}^2$, $R_n = 650 \text{ W/m}^2$, $U_g = 2.24 \text{ m/s}$ and $U_g = 1.5 \text{ m/s}$. T_a was fixed to $32 \text{ }^\circ\text{C}$. The solid line is the NWSB estimated empirically.

5. Concluding remarks

The detection of water stress in the field has been hampered by the uncertainty in determining the significance of point measurements of the actual field conditions. In addition, the number of point measurements collected is often limited by the time and cost of acquisition, reason that increases the uncertainty further. Options to spatially map water stress conditions in heterogeneous canopies, such as orchards, via remote sensing have been limited by the lack of spatial and temporal resolution of satellite-based approaches. This manuscript shows the feasibility for mapping two features directly related to the actual transpiration of olive orchards as affected by water deficits. Energy balance equations and the theoretical formulation of the CWSI have been combined with very high resolution thermal imagery to calculate G_c and CWSI for an heterogeneous olive canopy. Results showed their close relationship when calculated with standard approaches, demonstrating a successful validation against water potential and stomatal conductance field measurements. The ability to produce high resolution maps of G_c and CWSI, potentially used to calculate actual ET, and to be used as input for irrigation scheduling methods, respectively, provides a powerful tool for future applications of this methodology in the context of precision agriculture.

The potential use of new remote sensing methodologies based on active sensors could provide a better knowledge of the canopy structure (Moorthy et al., 2008), particularly on sparse canopies, and would help to refine the estimates of some of the parameters involved in this methodology, such as aerodynamic resistance and net radiation.

Acknowledgements

This work was funded by the Ministerio de Educación y Ciencia (MEC) of Spain with projects AGL-2003-01468, AGL2005-04049, EXPLORA-INGENIO AGL2006-26038-E/AGR, and CONSOLIDER CSD2006-67, as well as the Junta de Andalucía – with project AGR-595, and *in-kind* support provided by Bioiberica through project PETRI PET2005-0616. Technical support from UAV Navigation and Tetracam Inc. for accommodating airborne requirements are also acknowledged. V. González, M. Morales, C. Ruz, D. Notario, M. Guillén, C. Trapero, I. Calatrava, A. Vera and M. Ruiz Bernier are acknowledged for measurements and technical support in field and airborne campaigns. Special thanks to Dr. Luca Testi for his comments and support.

References

Baldocchi, D. D., Luxmoore, R. J., & Hatfield, J. L. (1991). Discerning the forest from the trees: An essay on scaling canopy stomatal conductance. *Agricultural and Forest Meteorology*, 54, 197–226.

Berk, A., Anderson, G., Acharya, P., Chetwynd, J., Bernstein, L., Shettle, E., et al. (1999). MODTRAN4 user's manual.

Berni, J. A. J., Zarco-Tejada, P. J., Suarez, L., & Fereres, E. (2009). Thermal and narrow-band multispectral remote sensing for vegetation monitoring from an unmanned aerial vehicle. *IEEE Transactions on Geoscience and Remote Sensing*, 47, 722–738.

Brest, C. L., & Goward, S. N. (1987). Deriving surface albedo measurements from narrow band satellite data. *International Journal of Remote Sensing*, 8, 351–367.

Brutsaert, W. (1975). On a derivable formula for long-wave radiation from clear skies. *Water Resources Research*, 11, 742–744.

Brutsaert, W. H. (1982). *Evaporation into the atmosphere: Theory, history, and applications*. Dordrecht: D. Reidel Publishing Co. p.

Cohen, Y., Alchanatis, V., Meron, M., Saranga, Y., & Tsipris, J. (2005). Estimation of leaf water potential by thermal imagery and spatial analysis. *Journal of Experimental Botany*, 56, 1843–1852.

Crawford, T. M., & Duchon, C. E. (1999). An improved parameterization for estimating effective atmospheric emissivity for use in calculating daytime downwelling longwave radiation. *Journal of Applied Meteorology*, 38, 474–480.

Fuchs, M., & Tanner, C. B. (1966). Infrared thermometry of vegetation. *Agronomy Journal*, 58, 297–601.

Furon, A. C., Warland, J. S., & Wagner-Riddle, C. (2007). Analysis of scaling-up resistances from leaf to canopy using numerical simulations. *Agronomy Journal*, 99, 1483–1491.

Glenn, D., Worthington, J., Welker, W., & McFarland, M. (1989). Estimation of peach-tree water-use using infrared thermometry. *Journal of the American Society for Horticultural Science*, 114, 737–741.

- Grant, O. M., Tronina, L., Jones, H. G., & Chaves, M. M. (2007). Exploring thermal imaging variables for the detection of stress responses in grapevine under different irrigation regimes. *Journal of Experimental Botany*, 58, 815–825.
- Herwitz, S., Johnson, L., Dunagan, S., Higgins, R., Sullivan, D., Zheng, J., et al. (2004). Imaging from an unmanned aerial vehicle: Agricultural surveillance and decision support. *Computers and Electronics in Agriculture*, 44, 49–61.
- Hipps, L., Asrar, G., & Kanemasu, E. (1985). A theoretically-based normalization of environmental effects on foliage temperature. *Agricultural and Forest Meteorology*, 35, 113–122.
- Hsiao, T. C., (1990) Measurements of plant water status. American Society of Agronomy, Madison (EUA); Crop Science Society of America, Madison (EUA); Soil Science Society of America, Madison (EUA).
- Idso, S. B. (1982). Non-water-stressed baselines: A key to measuring and interpreting plant water stress. *Agricultural Meteorology*, 27, 59–70.
- Idso, S., Jackson, R., & Reginato, R. (1978). Extending the 'degree-day' concept of plant phenological development to include water stress effects. *Ecology*, 59, 431–433.
- Idso, S., Jackson, R., Pinter, P. J. J., Reginato, R., & Hatfield, J. (1981). Normalizing the stress-degree-day parameter for environmental variability. *Agricultural Meteorology*, 24, 45–55.
- Iniesta, F., Testi, L., Orgaz, F., & Villalobos, F. J. (2009). The effects of regulated and continuous deficit irrigation on the water use, growth and yield of olive trees. *European Journal of Agronomy*, 30, 258–265.
- Jackson, R. D. (1982). Canopy temperature and crop water stress. *Advances in Irrigation*, 1, 43–85.
- Jackson, R., Reginato, R., & Idso, S. (1977). Wheat canopy temperature: A practical tool for evaluating water requirements. *Water Resources Research*, 13, 651–656.
- Jackson, R. D., Idso, S. B., Reginato, R. J., & Ehler, W. L. (1977). Crop temperature reveals stress. *Crop Soils*, 29, 10–13.
- Jackson, R., Idso, S., Reginato, R., & Pinter, P., Jr. (1981). Canopy temperature as a crop water stress indicator. *Water Resources Research*, 17, 1133–1138.
- Jackson, R. D., Kustas, W. P., & Choudhury, B. J. (1988). A reexamination of the crop water stress index. *Irrigation Science*, 9, 309–317.
- Jarvis, P. G. (1976). The interpretation of the variations in leaf water potential and stomatal conductance found in canopies in the field. *Philosophical Transactions of the Royal Society of London*, 273, 593–610.
- Jones, H. G. (1999). Use of infrared thermometry for estimation of stomatal conductance as a possible aid to irrigation scheduling. *Agricultural and Forest Meteorology*, 95, 139–149.
- Jones, H. G., Stoll, M., Santos, T., Sousa, C. D., Chaves, M. M., Grant, O. M. (2002). Use of infrared thermography for monitoring stomatal closure in the field: application to grapevine. *Journal of Experimental Botany*, 53, 2249–2260.
- Kjaerregaard, J. H., Plauborg, F. L., & Hansen, S. (2007). Comparison of models for calculating daytime long-wave irradiance using long term data set. *Agricultural and Forest Meteorology*, 143, 49–63.
- Leinonen, I., Grant, O. M., Tagliavia, C. P. P., Chaves, M. M., & Jones, H. G. (2006). Estimating stomatal conductance with thermal imagery. *Plant, Cell and Environment*, 29, 1508–1518.
- Lhomme, J. (1991). The concept of canopy resistance: Historical survey and comparison of different approaches. *Agricultural and Forest Meteorology*, 54, 227–240.
- Lhomme, J. P., & Monteny, B. (2000). Theoretical relationship between stomatal resistance and surface temperatures in sparse vegetation. *Agricultural and Forest Meteorology*, 104, 119–131.
- Liang, S. (2001). Narrowband to broadband conversions of land surface albedo I algorithms. *Remote Sensing of Environment*, 76, 213–238.
- Liu, S., Lu, L., Mao, D., & Jia, L. (2007). Evaluating parameterizations of aerodynamic resistance to heat transfer using field measurements. *Hydrology and Earth System Sciences*, 11, 769–783.
- Monteith, J. L., & Unsworth, M. H. (2008). *Principles of environmental physics*. Elsevier/Academic Press 440 pp.
- Moorthy, I., Miller, J. R., Baoxin, H., Chen, J., & Qingmou, L. (2008). Retrieving crown leaf area index from an individual tree using ground-base LIDAR data. *Canadian Journal of Remote Sensing*, 34, 320–332.
- Moran, M., Clarke, T., Inoue, Y., & Vidal, A. (1994). Estimating crop water deficit using the relation between surface-air temperature and spectral vegetation index. *Remote Sensing of Environment*, 49, 246–263.
- Moriana, A., & Fereres, E. (2002). Plant indicators for scheduling irrigation of young olive trees. *Irrigation Science*, 21, 83–90.
- Moriana, A., Villalobos, F. J., & Fereres, E. (2002). Stomatal and photosynthetic responses of olive (*Olea europaea* L.) leaves to water deficits. *Plant, Cell and Environment*, 25, 395–405.
- Möller, M., Alchanatis, V., Cohen, Y., Meron, M., Tsipris, J., Ostrovsky, V., et al. (2007). Use of thermal and visible imagery for estimating crop water status of irrigated grapevine. *Journal of Experimental Botany*, 58, 827–838.
- Nakayama, F. S., & Bucks, D. A. (1983). Application of a foliage temperature based crop water stress index to guayule (*Parthenium argentatum*). *Journal of Arid Environments*, 6, 269–276.
- Norman, J. M., Kustas, W. P., & Humes, K. S. (1995). Source approach for estimating soil and vegetation energy fluxes in observations of directional radiometric surface temperature. *Agricultural & Forest Meteorology*, 77, 263–293.
- Orgaz, F., Villalobos, F. J., Testi, L., & Fereres, E. (2007). A model of daily mean canopy conductance for calculating transpiration of olive canopies. *Functional Plant Biology*, 34, 178–188.
- Rana, G., & Kterji, N. (1998). A measurement based sensitivity analysis of the Penman-Monteith actual evapotranspiration model for crops of different height and in contrasting water status. *Theoretical and Applied Climatology*, 60, 141–149.
- Ritchie, J. T. (1972). Model for predicting evaporation from a row crop with incomplete cover. *Water Resources Research*, 8, 1204–1213.
- Salisbury, J. W., & D'Aria, D. M. (1992). Emissivity of terrestrial materials in the 8–14 μ m atmospheric window. *Remote Sensing of Environment*, 42, 83–106.
- Sepaskhah, A. R., & Kashefipour, S. M. (1994). Relationships between leaf water potential, CWSI, yield and fruit quality of sweet lime under drip irrigation. *Agricultural Water Management*, 25, 13–22.
- Sepulcre-Canto, G., Zarco-Tejada, P., Jimenez-Munoz, J., Sobrino, J., de Miguel, E., Villalobos, F. J. (2006). Detection of water stress in an olive orchard with thermal remote sensing imagery. *Agricultural and Forest Meteorology*, 136, 44.
- Sepulcre-Canto, G., Zarco-Tejada, P., Jimenez-Munoz, J., Sobrino, J., Soriano, M., Fereres, E., et al. (2007). Monitoring yield and fruit quality parameters in open-canopy tree crops under water stress. implications for aster. *Remote Sensing of Environment*, 107, 470.
- Shackel, K. A., Ahmadi, H., Biasi, W., Buchner, R., Goldhamer, D., Gurusingham, S., et al. (1997). Plant water status as an index of irrigation need in deciduous fruit trees. *HortTechnology*, 7, 23–29.
- Smith, R. C. G. (1988). Inferring stomatal resistance of sparse crops from infrared measurements of foliage temperature. *Agricultural and Forest Meteorology*, 42, 183–198.
- Sobrino, J., Jimenez-Munoz, J., Zarco-Tejada, P., Sepulcre-Canto, G., & de Miguel, E. (2006). Land surface temperature derived from airborne hyperspectral scanner thermal infrared data. *Remote Sensing of Environment*, 102, 115.
- Sugiura, R., Noguchi, N., & Ishii, K. (2005). Remote-sensing technology for vegetation monitoring using an unmanned helicopter. *Biosystems Engineering*, 90, 369–379.
- Tanner, C. B. (1963). Plant temperatures. *Agronomy Journal*, 55, 210–211.
- Testi, L., Villalobos, F. J., & Orgaz, F. (2004). Evapotranspiration of a young irrigated olive orchard in Southern Spain. *Agricultural and Forest Meteorology*, 121, 1–18.
- Testi, L., Orgaz, F., & Villalobos, F. J. (2006). Variations in bulk canopy conductance of an irrigated olive (*Olea europaea* L.) orchard. *Environmental and Experimental Botany*, 55, 15–28.
- Testi, L., Goldhamer, D. A., Iniesta, F., & Salinas, M. (2008). Crop water stress index is a sensitive water stress indicator in pistachio trees. *Irrigation Science*, 26, 395–405.
- Verhoef, A., McNaughton, K. G., & Jacobs, A. F. G. (1997). A parameterization of momentum roughness length and displacement height for a wide range of canopy densities. *Hydrology and Earth System Sciences*, 1, 81–91.
- Villalobos, F. J., Orgaz, F., & Testi, L. (2000). Measurement and modeling of evapotranspiration of olive (*Olea europaea* L.) orchards. *European Journal of Agronomy*, 13, 155–163.
- Viney, N. R. (1991). An empirical expression for aerodynamic resistance in the unstable boundary layer. *Boundary-Layer Meteorology*, 56, 381–393.
- Wanjura, D. F., Hatfield, J. L., & Upchurch, D. R. (1990). Crop water stress index relationships with crop productivity. *Irrigation Science*, 11, 93–99.
- Yazar, A., Howell, T. A., Dusek, D. A., & Copeland, K. S. (1999). Evaluation of crop water stress index for LEPA irrigated corn. *Irrigation Science*, 18, 171–180.